Applicability of Dynamic Mode Decomposition to Estimate Fundamental Mode Component of Prompt Neutron Decay Constant from Experimental Data

Fuga Nishioka[a]*, Tomohiro Endo[a], Akio Yamamoto[a], Masao Yamanaka[b †], Cheol Ho Pyeon[b]

[a]*Nagoya University, Graduate School of Engineering, Department of Applied Energy, Nagoya, Japan*

[b]*Kyoto University, Institute for Integrated Radiation and Nuclear Science, Osaka, Japan*

Corresponding author: Fuga Nishioka

*E-mail: f-nishioka@fermi.energy.nagoya-u.ac.jp

Address: Nagoya University, Furo-cho, Chikusa-ku, Nagoya, Japan, 464-8603

Tel, Fax: +81-52-789-3775, +81-52-789-3608

Number of Pages: 19

Number of Tables: 2

Number of Figures: 6

† Present affiliation: *Nuclear Engineering, Ltd., Osaka, Japan*

ABSTRACT

To robustly estimate the fundamental mode component of prompt neutron decay constant α in a subcritical system, dynamic mode decomposition (DMD) is applied to time-series data obtained by the pulsed-neutron source (PNS) and Rossi-α methods. For the statistical uncertainty quantification of α by DMD, randomly sampled virtual data are used for the DMD procedure. The applicability of DMD is demonstrated by analyzing the experimental results by the PNS and Rossi-α methods, which are performed at the Kyoto University Critical Assembly (KUCA). When applying the DMD to the PNS and Rossi-α experimental data, a constant signal was added to the experimental data to remove the background constant component. The application results indicate that DMD enables one to robustly estimate the fundamental mode component of α in the PNS and Rossi-α methods.

KEYWORDS: prompt neutron decay constant, dynamic mode decomposition, fundamental mode component, pulsed-neutron source method, Rossi-α method

I. INTRODUCTION

The prompt neutron decay constant α is a time constant that represents the exponential decay of the number of prompt neutrons in a subcritical system. The experimental value of the fundamental mode component of α is useful for estimating the subcriticality of the measurement system and reducing nuclear data-induced uncertainties in numerical results using data assimilation [1]. The fundamental mode component shows the slowest decay among those of higher mode components obtained by the time-dependent prompt neutron transport equation. Therefore, when sufficient time has elapsed after a source neutron is generated, the fundamental mode component becomes the most dominant component of the neutron flux in the system.

The pulsed neutron source (PNS) method [2] and the Rossi-α method [3] can be applied to obtain the α value experimentally. In the PNS method, the time variation of neutron count rates in the subcritical system is measured by periodically injecting pulsed neutrons into the subcritical system. After pulsed neutrons are injected into the subcritical system, the neutron count rates temporarily increase due to the neutron transport and the fission chain reaction caused by the pulsed neutrons. Subsequently, since the fission chain reaction terminates in the subcritical system, the neutron count rates exponentially decrease by a system-specific decay constant. The system-specific decay constant corresponds to α. By contrast, in the Rossi-α method, the reactor noise signals in the subcritical system are measured to obtain a histogram of the neutron-detection-time intervals. The histogram of the neutron-detection-time intervals corresponds to the time variation of the probability that a neutron pair belonging to the same fission chain system is detected. The probability also decreases exponentially by the prompt neutron decay constant α. Generally, the value of α is estimated by the least-squares fitting method using an exponential function to the measured time-series data of the PNS or Rossi-α method.

The problem of the least-squares fitting method is that the estimated α contains a systematic error derived from the higher mode components because a precise extraction of only the fundamental mode component is difficult. To reduce the influence of higher mode components, the time-series data obtained by the PNS or Rossi-α method within a masking time interval are excluded in the conventional least-squares fitting. In other words, the estimated value of α depends on the masking time. To address this issue, Katano proposed linear combination method [4–6]. In this method, the time-series data acquired using multiple detectors are summed with the weighting coefficients, to be expressed as a single exponential decay as much as possible. However, not only the value of α but also the weighting coefficients should be determined by the nonlinear least-squares fitting. Hence, the initial values of these fitting parameters must be assigned appropriately to estimate the fundamental mode component of α, i.e., there is an issue to set the initial values of these fitting parameters automatically.

To overcome this issue, we aim to develop another method that can robustly estimate the fundamental mode component of α without requiring any initial values in the conventional fitting process. For this purpose, this study focused on dynamic mode decomposition (DMD). DMD is a data-driven method that can extract the spatio-temporal structure of a system from time-series data obtained from experiments or numerical simulations [7]. Recently, DMD has been investigated in the field of reactor physics, e.g., to construct the reduced order models of kinetic properties in subcritical systems [8]. In DMD, the time constant for each mode can be obtained by decomposing the time-series data into a summation of exponential modes. Since the experimental results obtained by the PNS and Rossi-α methods can also be expressed by the summation of exponential functions, the applicability of DMD to both methods is expected. Furthermore, unlike conventional fitting and linear combination methods, DMD does not require any initial values, i.e., the fundamental mode component of α can be uniquely determined from the time constant obtained by applying DMD. In this study, the applicability of DMD for extracting the fundamental mode component of α from actual experimental results by the PNS and Rossi-α methods was investigated.

The remainder of this paper is organized as follows. In Section II, the theoretical formulas of the PNS and Rossi-α methods are briefly explained. Subsequently, the theory of DMD is presented, followed by a procedure to estimate the statistical uncertainty of α by DMD using randomly sampled virtual data. Section III describes the PNS and Rossi-α experiments performed at the Kyoto University Critical Assembly (KUCA) and presents the application results of DMD for each experiment. Finally, concluding remarks are presented in Section IV.

II. THEORY

II.A. Pulsed-Neutron Source and Rossi-α Methods

In the PNS method, pulsed neutrons are periodically injected into the subcritical system, and then the time variation in the neutron count rate $C(t)$ is measured. The prompt neutron decay constant α is estimated by analyzing the exponential time variation of $C(t)$.

The theoretical formula for the neutron flux after pulsed neutrons are injected into a subcritical system is explained briefly below. First, let us define Green's function $G\left(\vec{r},E,\vec{\Omega},t|\vec{r}_0,E_0,\vec{\Omega}_0,t_0\right)$ as the neutron flux at $\left(\vec{r},E,\vec{\Omega},t\right)$ after injecting one neutron into the system at $\left(\vec{r}_0,E_0,\vec{\Omega}_0,t_0\right)$. Here, $\vec{r}$, E, $\vec{\Omega}$, and t represent the position, neutron energy, neutron flight direction, and time variables, respectively; the subscript 0 indicates the index for neutron injection. By focusing on the time domain where the decay of prompt neutron component is dominant, the Green's function $G\left(\vec{r},E,\vec{\Omega},t|\vec{r}_0,E_0,\vec{\Omega}_0,t_0\right)$ can be expanded using the α-eigenfunction as follows [9]:

$$G\left(\vec{r},E,\vec{\Omega},t|\vec{r}_0,E_0,\vec{\Omega}_0,t_0\right)=\sum_{n=0}^{\infty}\psi_n\left(\vec{r},E,\vec{\Omega}\right)\psi_n^{\dagger}\left(\vec{r}_0,E_0,\vec{\Omega}_0\right)e^{-\alpha_n(t-t_0)}, \tag{1}$$

where ψ_n and $\psi_n^{\dagger}$ represent the forward and adjoint eigenfunctions, respectively. These eigenfunctions satisfy the following forward and adjoint prompt-α eigenvalue equations using the conventional nomenclature in the reactor physics:

$$\mathbf{B}\psi_n\left(\vec{r},E,\vec{\Omega}\right)=\frac{\alpha_n}{\mathrm{v}(E)}\psi_n\left(\vec{r},E,\vec{\Omega}\right), \tag{2}$$

$$\mathbf{B}^{\dagger}\psi_n^{\dagger}\left(\vec{r},E,\vec{\Omega}\right)=\frac{\alpha_n}{\mathrm{v}(E)}\psi_n^{\dagger}\left(\vec{r},E,\vec{\Omega}\right), \tag{3}$$

where vacuum conditions are assumed for ψ_n and $\psi_n^{\dagger}$ at the outer boundary conditions; $\mathbf{B}$ and $\mathbf{B}^{\dagger}$ are the forward and adjoint Boltzmann operators, respectively, defined as follows:

$$\begin{aligned}\mathbf{B}\equiv\vec{\Omega}\cdot\nabla+\Sigma_{\mathrm{t}}(\vec{r},E)-\int_0^{\infty}dE'\int_{4\pi}d\Omega'\,\Sigma_{\mathrm{s}}\left(\vec{r},E'\to E,\vec{\Omega}'\to\vec{\Omega}\right)\\-\frac{\chi_{\mathrm{p}}(\vec{r},E)}{4\pi}\int_0^{\infty}dE'\int_{4\pi}d\Omega'\,\nu_{\mathrm{p}}\Sigma_{\mathrm{f}}(\vec{r},E'),\end{aligned} \tag{4}$$

$$
\begin{aligned}
\mathbf{B}^{\dagger} \equiv -\vec{\Omega}\cdot\nabla + \Sigma_{\mathrm{t}}(\vec{r},E) - \int_0^{\infty} dE' \int_{4\pi} d\Omega'\, \Sigma_{\mathrm{s}}\big(\vec{r},E \to E',\vec{\Omega} \to \vec{\Omega}'\big) \\
- \nu_{\mathrm{p}}\Sigma_{\mathrm{f}}(\vec{r},E) \int_0^{\infty} dE' \int_{4\pi} d\Omega' \frac{\chi_{\mathrm{p}}(\vec{r},E')}{4\pi}.
\end{aligned}
\tag{5}
$$

To derive the theoretical formula of the PNS method, let us assume that delta-functional neutrons q_{PNS} are repeatedly injected with a constant period T_0 at time $t = -iT_0$ ($i = 0,1,2,\cdots$). In the steady-state after sufficient time from the start of pulsed neutron injection, an approximately constant background neutron source q_{BG} exists in the system because of the inherent neutron source (e.g., spontaneous fission and (α, n) reaction) in the nuclear fuel and the decay of delayed neutron precursors. Hence, the total neutron source $q(\vec{r},E,\vec{\Omega},t)$ in the system can be expressed as follows:

$$
q(\vec{r},E,\vec{\Omega},t) = q_{\mathrm{PNS}}(\vec{r},E,\vec{\Omega})\left(\sum_{i=0}^{\infty}\delta(t-iT_0)\right) + q_{\mathrm{BG}}(\vec{r},E,\vec{\Omega}). \tag{6}
$$

Based on Eqs. (1) and (6), the time variation of the neutron flux $\psi(\vec{r},E,\vec{\Omega},t)$ due to the PNS can be derived by integrating the product of Green's function $G(\vec{r},E,\vec{\Omega},t|\vec{r}_0,E_0,\vec{\Omega}_0,t_0)$ and $q(\vec{r},E,\vec{\Omega},t)$ as follows:

$$
\begin{aligned}
&\psi(\vec{r},E,\vec{\Omega},t) \\
&= \int_V dV_0 \int_0^{\infty} dE_0 \int_{4\pi} d\Omega_0 \int_{-\infty}^{t} dt_0\, q(\vec{r}_0,E_0,\vec{\Omega}_0,t_0) G(\vec{r},E,\vec{\Omega},t|\vec{r}_0,E_0,\vec{\Omega}_0,t_0) \\
&= \sum_{n=0}^{\infty} F_n(\vec{r},E,\vec{\Omega}) e^{-\alpha_n t} + F_{\mathrm{BG}}(\vec{r},E,\vec{\Omega}),
\end{aligned}
\tag{7}
$$

where F_n and F_{BG} represent the n'th order expansion coefficient and the background component, respectively. Finally, the time variation of the neutron count rate $C(t)$ in the PNS method can be derived by integrating the product of the macroscopic detection cross section Σ_{d} and the neutron flux $\psi(\vec{r},E,\vec{\Omega},t)$ over the total phase space:

$$
C(t) = \langle \Sigma_{\mathrm{d}} \psi \rangle = \sum_{n=0}^{\infty} C_n e^{-\alpha_n t} + C_{\mathrm{BG}}, \tag{8}
$$

where

$\langle\ \rangle$ = total integral over the total phase space

C_n = n'th order expansion coefficient

C_{BG} = constant background component.

As shown in Eq. (8), the theoretical formula for the neutron count rate $C(t)$ in the PNS method can be expressed by the sum of the exponential higher mode components and the constant component [5,6].

By contrast, the Rossi-α method is one of the reactor noise analysis methods. First, the reactor noise (i.e., time-series data of neutron-detection time) in the subcritical system in steady-state condition is measured. Subsequently, the histogram $P(\tau)$ of the neutron-detection-time interval τ is obtained by analyzing two detection time points. Namely, the time interval τ is calculated for each combination of all neutron pairs detected within the measurement time, and the histogram $P(\tau)$ is counted to estimate the prompt neutron decay constant α.

The theoretical formula for the histogram $P(\tau)$ is briefly explained below. Let us consider a subcritical system in which the steady-state is maintained by an external neutron source. Based on the heuristic method with Green's function expressed in Eq. (1) [9,10], the theoretical formula for $P(\tau)$ can be derived from the α-eigenfunction expansion as follows:

$$P(\tau) = \sum_{n=0}^{\infty} P_n e^{-\alpha_n \tau} + P_{\mathrm{u}}, \tag{9}$$

where

P_n = n'th order expansion coefficient

P_{u} = uncorrelated term representing the frequency due to independent neutron pairs that do not belong to the same fission chain.

As shown in the experimental results of the Rossi-α method in Section III.C., according to the experimental condition, the uncorrelated term P_{u} in Eq. (9) can be regarded as an almost constant term. In such a case, as in the same manner as the PNS method, the theoretical formula for the histogram $P(\tau)$ in the Rossi-α method can be also expressed by the sum of the exponential higher mode components and the constant component.

II.B. Dynamic Mode Decomposition

Let us consider that neutrons are successively counted by n time steps of time interval Δt using m neutron detectors in the PNS method. Alternatively, in the Rossi-α method, let us consider that the frequency of the neutron-detection-time interval τ is measured by n bins of time interval $\Delta\tau$ using m neutron detectors. The discrete time-series data of the PNS or Rossi-α measurement are arranged into an $m \times n$ matrix $\mathbf{X}$, where $m < n$. By taking the i'th through j'th time-series data from the original matrix $\mathbf{X}$, a slicing matrix $\mathbf{X}_{\boldsymbol{i:j}}$ of size $m \times (j - i + 1)$ is constructed. Based on two slicing matrices $\mathbf{X}_{\mathbf{1}:\boldsymbol{n}-\mathbf{1}}$ and $\mathbf{X}_{\mathbf{2}:\boldsymbol{n}}$, the time evolution matrix $\mathbf{A}$ in the DMD satisfies the following equation **[7]**:

$$\mathbf{A}\mathbf{X}_{\mathbf{1}:\boldsymbol{n}-\mathbf{1}} \approx \mathbf{X}_{\mathbf{2}:\boldsymbol{n}} \,. \tag{10}$$

For Eq. (10), it is assumed that the time variation of the time-series data is exponential. The time evolution matrix $\mathbf{A}$ transforms each time-step data into the next time-step data. In the DMD, the time evolution matrix $\mathbf{A}$ can be estimated from the time-series data only.

The procedure to calculate the time evolution matrix $\mathbf{A}$ is briefly explained below. First, $\mathbf{X}_{\mathbf{1}:\boldsymbol{n}-\mathbf{1}}$ is decomposed into three matrices using singular value decomposition as follows:

$$\mathbf{X}_{\mathbf{1}:\boldsymbol{n}-\mathbf{1}} = \mathbf{U}\mathbf{\Sigma}\mathbf{V}^{*}, \tag{11}$$

where

matrix $\mathbf{U} = m \times m$ unitary matrix

matrix $\mathbf{\Sigma} = m \times m$ diagonal matrix with diagonal elements corresponding to singular values

matrix $\mathbf{V} = (n - 1) \times m$ unitary matrix

superscript $* =$ denotes a complex conjugate transposition.

Using Eq. (11), the pseudo-inverse matrix $\mathbf{X}^{+}_{\mathbf{1}:\boldsymbol{n}-\mathbf{1}}$ can be obtained as follows:

$$\mathbf{X}^{+}_{\mathbf{1}:\boldsymbol{n}-\mathbf{1}} = \mathbf{V}\mathbf{\Sigma}^{-1}\mathbf{U}^{*}, \tag{12}$$

where superscript -1 indicates the inverse matrix. By multiplying both sides of Eq. (10) by the pseudo-inverse matrix $\mathbf{X}^{+}_{\mathbf{1}:\boldsymbol{n}-\mathbf{1}}$ from the right, the time evolution matrix $\mathbf{A}$ can be obtained as follows:

$$\mathbf{A} = \mathbf{X}_{\mathbf{2}:\boldsymbol{n}}\mathbf{V}\mathbf{\Sigma}^{-1}\mathbf{U}^{*}. \tag{13}$$

By applying the eigenvalue decomposition to the estimated $\mathbf{A}$, eigenvalues λ_i and eigenvectors $\psi_i(\vec{r})$ associated with the matrix $\mathbf{A}$ are obtained for each mode ($1 \leq i \leq m$). Note that $\psi_i(\vec{r})$ exhibits a discretized form in the space. Using the eigenvectors $\psi_i(\vec{r})$, the time-series data of $f(\vec{r}, t)$ at position $\vec{r}$ can be expanded as follows:

$$f(\vec{r},t) = \sum_{i=1}^{m} a_i \psi_i(\vec{r}) \exp(\omega_i t)\,, \tag{14}$$

where a_i and ω_i are the amplitude (or expansion coefficient) and time constant of the i'th mode, respectively. The time constant ω_i can be calculated using the following formula:

$$\omega_i = \frac{\ln(\lambda_i)}{\Delta t}. \tag{15}$$

Note that the prompt neutron decay constant is a negative time constant and that the sign of α is opposite to that of ω_i, i.e., $\alpha_i = -\omega_i$. In addition, the fundamental mode component of α is the slowest decay constant except for the constant background component C_{BG} in Eq. (8) or P_{u} in Eq. (9) as explained in Sec. II.A. The constant component degrades the estimation accuracy of the fundamental mode component of α. To remove the contribution of the constant background component, a constant signal for all time steps is added virtually to matrix **X**. By adding a constant signal, the constant background component can be extracted as an independent mode, which contains the first maximum eigenvalue $\lambda_{\max} = 1$, because the background component corresponds to $\exp\left(-\frac{\ln(\lambda_{max})}{\Delta t} t\right) = 1$. Consequently, the fundamental mode component of α is determined by the second maximum eigenvalue except for the first maximum eigenvalue $\lambda_{\max} = 1$ as follows:

$$\alpha = -\frac{\ln\big(\max(\lambda_{i'})\big)}{\Delta t} \text{ where } \lambda_{i'} < \lambda_{\max}\,. \tag{16}$$

II.C. Evaluation of Statistical Uncertainty of α Using Randomly Sampled Virtual Data

Since the measured time-series data contain statistical errors, the random sampling method [11] was utilized to evaluate the statistical uncertainty of α in the DMD procedure. N virtual time-series data sets were sampled by adding normal random numbers to the elements in matrix **X**. Here, the element of matrix **X** in the i'th row and j'th column is denoted by x_{ij}. In the PNS method, x_{ij} corresponds to the neutron counts measured by the i'th neutron detector at the j'th time step. By contrast, in the Rossi-α method, x_{ij} corresponds to the frequency of the neutron-detection-time interval measured by the i'th neutron detector at the j'th time interval. If each x_{ij} has a statistical uncertainty σ_{ij}, then the k'th virtual time series data $\mathbf{X}^{(k)}$ is generated via perturbation as follows:

$$x_{ij}^{(k)} = x_{ij} + \sigma_{ij}\mathcal{N}(0,1)\,, \tag{17}$$

where $\mathcal{N}(0,1)$ is the standard normal random number. By applying repeatedly DMD to each virtual data set, a histogram of α can be obtained. Figure 1 shows a typical example of a histogram for α. Based on the obtained histogram of α, the sample mean and unbiased standard deviation of α were estimated. The estimated standard deviation corresponds to the statistical uncertainty of α in the DMD procedure. The procedure for calculating α with statistical uncertainty is summarized as follows:

1. Create k'th perturbed virtual time-series data by adding normal random numbers to matrix $\mathbf{X}^{(k)}$.
2. Calculate time evolution matrix $\mathbf{A}^{(k)}$ based on slicing matrices $\mathbf{X}_{\mathbf{1}:\boldsymbol{n}-\mathbf{1}}^{(k)}$ and $\mathbf{X}_{\mathbf{2}:\boldsymbol{n}}^{(k)}$.
3. Obtain eigenvalue $\lambda_i^{(k)}$ for each mode by eigenvalue decomposition of matrix $\mathbf{A}^{(k)}$.
4. Evaluate the fundamental mode component of the prompt neutron decay constant $\alpha^{(k)}$ using Eq. (16).
5. Repeat steps 1–4 N times to obtain the histogram of α.
6. Estimate the sample mean and standard deviation of α by statistical processing for the obtained histogram of α.

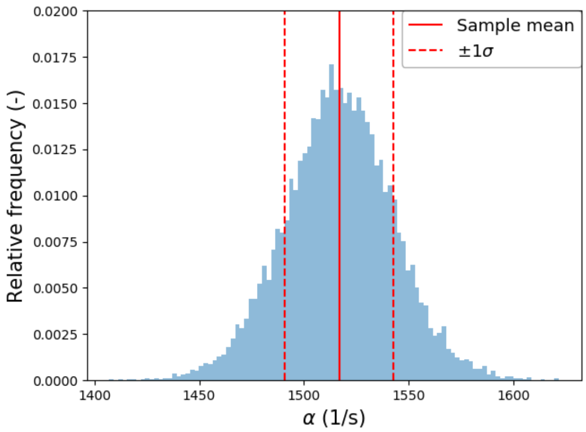

Figure 1. Example of histogram for α by randomly sampled virtual data.

III. APPLICATION TO KUCA EXPERIMENT

III.A. Experimental Conditions

The experimental KUCA core is shown in Fig. 2. All control rods (C1, C2, and C3) and safety rods (S4, S5, and S6) were fully inserted into the core in this experiment. Figure 3 shows the configurations of the fuel assemblies loaded in the core. The 1/8”p60EUEU and 1/8”p10EUEU fuel assemblies were configured by a unit fuel-cell #1, which comprised two 1/16” enriched uranium plates and one 1/8” polyethylene plate. By contrast, the EU-Al-NU-Al-EU fuel assembly was configured by two different unit fuel-cells #1 and #3. Unit cell #3 comprised one natural uranium plate, four 1/16” enriched uranium plates, and four Al plates.

In this experiment, 100-MeV protons generated from the fixed-field alternating gradient (FFAG) accelerator were periodically injected onto the Pb-Bi target. Therefore, spallation reactions generated pulsed neutrons periodically. The beam injection period of the FFAG accelerator was 30 Hz. Using 10 neutron detectors (four BF_3 detectors #1–#4, four fiber-optic detectors #1–#4, two fission chambers #1–#2), the time-series data of neutron counts were measured for 1,000 s after the core reached the steady-state. In order to successfully apply DMD to the experimental data, many combinations of neutron flux with various higher mode components are necessary. Thus, as shown in Fig. 2, the detectors were dispersed in asymmetrical positions to obtain the various higher mode components. In the PNS method, we analyzed the neutron count rates per one pulsed neutron-shot and the statistical uncertainties using the 30,000(=30 Hz $\times$ 1,000 s) pulsed neutron-injection results. The statistical uncertainty of the neutron count rate was evaluated by the central limit theorem. In the Rossi-α method, the histogram $P(\tau)$ was obtained as the mean value of several histograms generated from the measurement results of the reactor noise for 1,000 s. Similar to the PNS experiment, the statistical uncertainty of $P(\tau)$ was also evaluated by the central limit theorem.

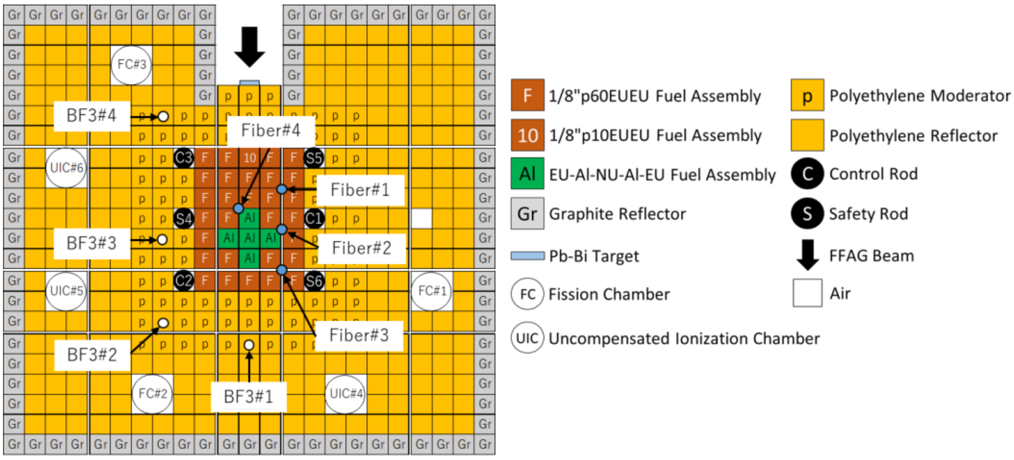

Figure 2. Top view of experimental core.

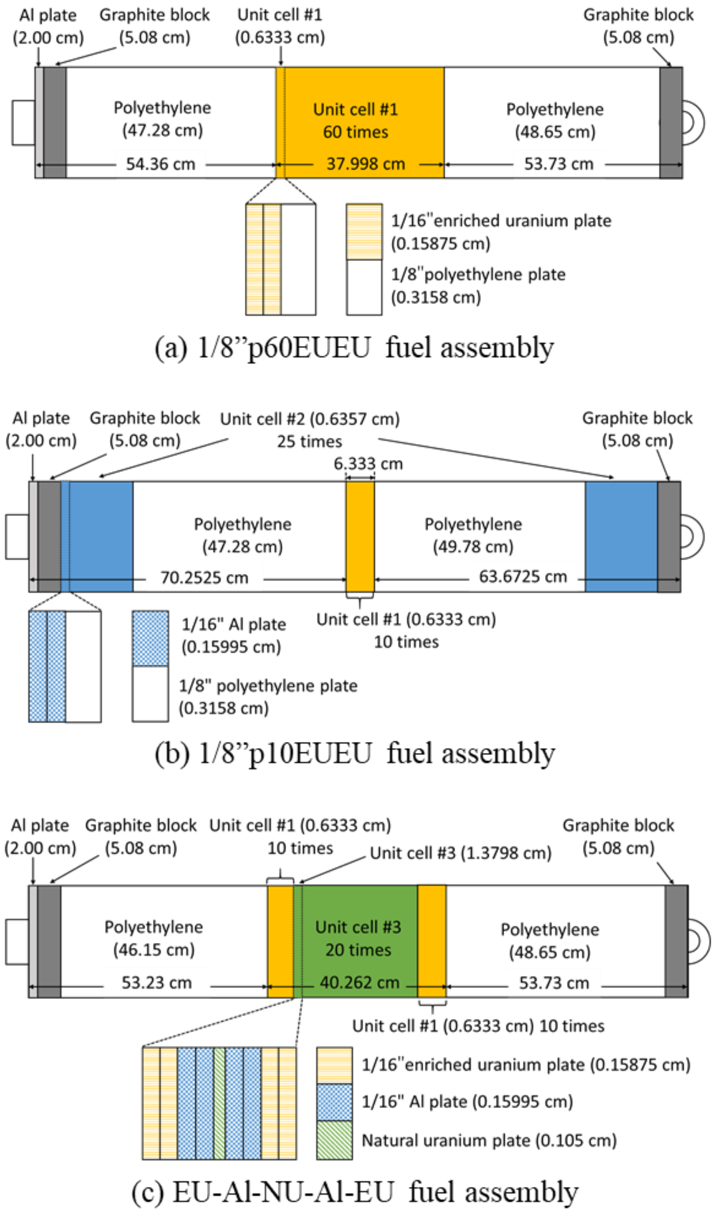

Figure 3. Configurations of fuel assemblies.

Table 1 shows the control rod worth measured by the rod drop method [12] and the excess reactivity of the experimental core measured by the positive period method [12]. To evaluate the rod worth and excess reactivity, the decay constants λ_i and the relative yields a_i for delayed neutrons were taken from the Keepin data [13]. As shown in Fig. 2, the control rods and safety rods were arranged symmetrically. Therefore, it was assumed that the rod worth of the safety rod was equal to that of the control rod at the symmetric position. Table 1 also shows the subcriticality $(-\rho)$ of the experimental core calculated from the rod worth and the excess reactivity. The uncertainty of each value presented in Table 1 was evaluated using the random sampling method [11] to consider the normal-distributed uncertainties of λ_i, a_i [13] and the measured doubling time, as well as Poisson-distributed statistical errors of neutron counts in the rod drop method. In the random sampling method, the sum of the perturbed a_i was normalized to unity, and the sample size was set to 10,000 to estimate the uncertainties of the rod worth, excess reactivity, and $(-\rho)$.

Table 1. Experimental results of rod drop method and period method.

Rod worth ($)	C1, S4	1.203 ± 0.041
	C2, S6	0.408 ± 0.014
	C3, S5	0.408 ± 0.014
Excess reactivity ($)		0.036 ± 0.001
Subcriticality $(-\rho)$ ($)		4.001 ± 0.133

Table 2 shows the effective delayed neutron fraction β_{eff} and the neutron generation time Λ for the experimental core calculated by MCNP6.2 [14] with ENDF/B-VII.1 [15]. In Table 2, the uncertainties in β_{eff} and Λ are the statistical errors due to MCNP6.2. Based on the fundamental mode approximation, the prompt neutron decay constant α assumed to be nearly equal to $(\beta_{\mathrm{eff}} - \rho)/\Lambda$. For comparison with the measured α, Table 2 also presents the value of $(\beta_{\mathrm{eff}} - \rho)/\Lambda$ using the experimental result of $(-\rho)$ and the numerical results of Λ and β_{eff}. Similar to Table 1, the uncertainty of $(\beta_{\mathrm{eff}} - \rho)/\Lambda$ was evaluated using the random sampling method.

Table 2. Calculation results of point kinetics parameters and $(\boldsymbol{\beta}_{\mathbf{eff}} - \boldsymbol{\rho})/\boldsymbol{\Lambda}$.

Effective delayed neutron fraction β_{eff} (-)	0.00797 ± 0.00006
Neutron generation time Λ (μs)	27.20 ± 0.04
$(\beta_{\mathrm{eff}} - \rho)/\Lambda$ (1/s)	1466 ± 39

III.B. Experimental Results and DMD Analysis

The time-series data of the PNS and Rossi-α methods were successively measured using 10 neutron detectors (four BF_3 detectors, four fiber-optic detectors, and two fission chambers). The positions of the detectors in the experimental core are shown in Fig. 2. In the PNS method, neutrons were successively counted by a time step of $\Delta t = 0.0001$ (s). In the Rossi-α method, the frequency of neutron-detection-time interval was also calculated by a time bin of $\Delta\tau = 0.0001$ (s). Figure 4 shows the experimental results obtained by the PNS and Rossi-α methods. In the DMD, matrices **X** was constructed using both time-series data shown in Fig. 4, respectively. From Fig. 4-(a), the size of the matrix **X** in the PNS method was 10×333, i.e., 333 time steps were measured with 10 neutron detectors. Meanwhile, from Fig. 4-(b), the size of matrix **X** in the Rossi-α method was 10×200, i.e., 200 time intervals were measured with 10 neutron detectors. In addition, constant signals of 1 for all time steps were virtually added to both matrices **X**, in order to remove the constant components shown in Eqs. (8) and (9) in the DMD procedure.

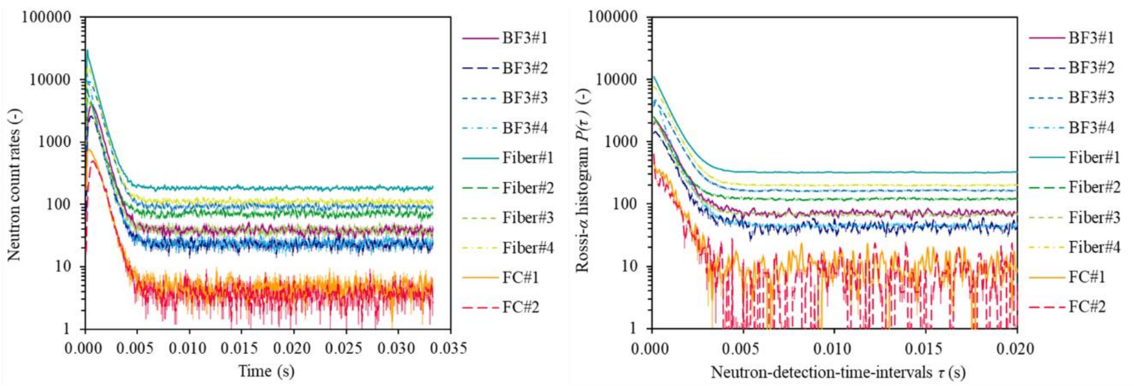

(a) PNS histograms (b) Rossi-α histograms

Figure 4. Experimental results of the PNS and Rossi-α method.

Figure 5 shows the results of applying DMD and the conventional fitting method to the PNS method. Similarly, Fig. 6 shows the results of applying the aforementioned methods to the Rossi-α method. The horizontal axes in Figs. 5 and 6 represent the masking time for excluding the effect of higher mode components. For comparison, the calculated $(\beta_{\text{eff}} - \rho)/\Lambda$ value shown in Table 2 is also presented in Figs. 5 and 6. In the conventional fitting method, the PNS and Rossi-α histograms shown in Fig. 4 were fitted by the following formulas, respectively:

$$C(t) = C_0 \exp(-\alpha t) + C_{\mathrm{BG}}\,, \tag{18}$$

$$P(\tau) = P_0 \exp(-\alpha \tau) + P_{\mathrm{u}}\,, \tag{19}$$

where C_0, C_{BG}, P_0, and P_{u} are fitting parameters, and α is the prompt neutron decay constant. To obtain the least-squares fitting results shown in Figs 5-(a) and 6-(a), the "scipy.optimize.curve_fit" module [16] was utilized. By setting the option of "absolute_sigma" to "True," the fitting error of α was evaluated using the absolute value of the statistical uncertainty (1σ) at each time step. Note that the fitting error in this study was approximately estimated without considering the covariance between the different time steps. Hence, the fitting errors of α shown in Fig. 5-(a) and Fig. 6-(a) were underestimated, compared with the bias between the fitting result and $(\beta_{\mathrm{eff}} - \rho)/\Lambda$. By contrast, in the DMD, the fundamental mode component of α and the statistical uncertainty were estimated as described in Sec. II.C. The sample size N for evaluating the statistical uncertainty of α was set as $N = 10{,}000$ such that the relative statistical error of the uncertainty estimated by the random sampling method was less than 1 %. When $N = 10{,}000$, the relative statistical error of the uncertainty using the random sampling method is expected to be $1/\sqrt{2(N-1)} \approx 0.7$ % [17].

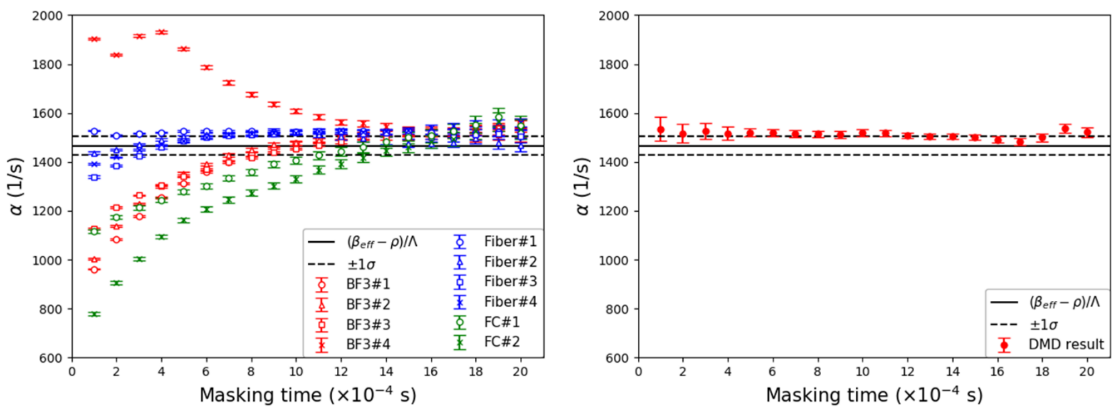

(a) Conventional fitting results (b) DMD result

Figure 5. Estimation results of α by PNS method.

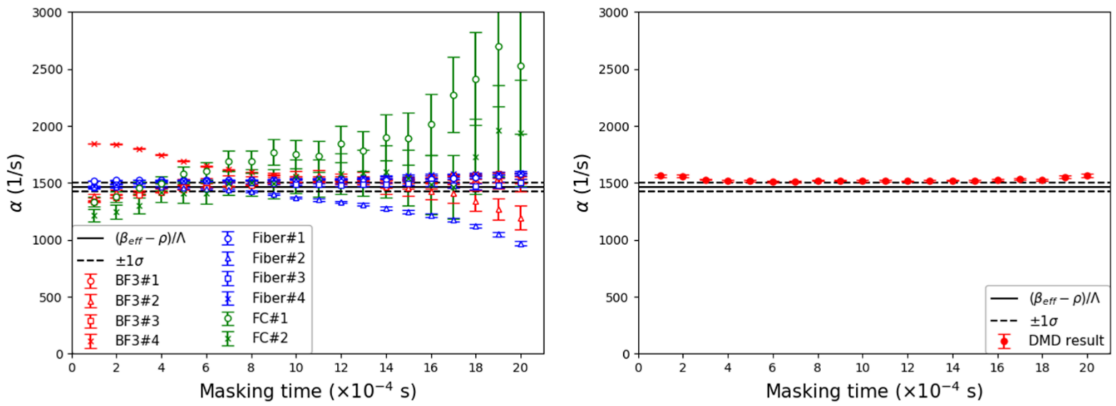

(a) Conventional fitting results (b) DMD result

Figure 6. Estimation results of α by Rossi-α method.

III.C. Discussion

In the early stage of the time steps of the PNS and Rossi-α histograms, the higher mode components do not necessarily decay sufficiently. Using the conventional fitting method, the effect of the higher mode component becomes significant in the early stage of decay. For example, in the case of the PNS method as shown in Fig. 5-(a), the conventional fitting results of the BF_3 detectors and fission chambers deviated significantly from the $(\beta_{\text{eff}} - \rho)/\Lambda$ value as the masking time decreased. Also in the case of the Rossi-α method as shown in Fig. 6-(a), a similar trend was also observed for the BF_3 detectors and fission chambers. These differences between the conventional fitting results and the $(\beta_{\text{eff}} - \rho)/\Lambda$ value were greater than the fitting error of α, i.e., the conventional fitting results contained large systematic errors due to the higher mode components in the early stages of decay.

Meanwhile, for the Rossi-α method, as the masking time increased, the fitting results of α for BF_3#2, Fiber#2, and fission chambers deviated from the $(\beta_{\text{eff}} - \rho)/\Lambda$ value, as shown in Fig. 6-(a). This is because the decay of the fundamental mode component could not be easily extracted when the masking time to eliminate the effect of higher mode components was too large, i.e, the histograms after masking were almost constant. Furthermore, the larger variations in the fitting results of α for FC#1 and FC#2 with respect to the masking time were observed due to the larger statistical uncertainties of the Rossi-α histograms for FC#1 and FC#2, as shown in Fig. 4-(b).

As discussed above, the appropriate masking time must be carefully selected to appropriately estimate the fundamental mode component of α using the conventional fitting method. However, the determination of masking time is difficult because the reference value of α is usually unknown beforehand. In addition, since multiple detectors were used in this experiment, the conventional fitting method yielded different estimation results of α for each detector, i.e., the selection of an appropriate detector to obtain the fundamental mode component of α was not straightforward. To summarize, in the conventional fitting method, it is difficult to uniquely determine the value of α only from the measurement results.

By contrast, in DMD, the influence of higher mode components could be eliminated from the fundamental mode component by decomposing the time-series data into multiple exponential modes. Therefore, even in the early stages of decay, the fundamental mode component of α can be extracted robustly. Consequently, the variation in the estimated α with respect to the masking time could be reduced significantly, as shown in Figs. 5-(b) and 6-(b). DMD enables us to robustly estimate the fundamental mode component of α even when the reference value is unknown. The masking time in DMD can be determined simply to minimize the statistical uncertainty of α. For example, the DMD results of α with the smallest statistical uncertainty were 1505 ± 10 (1/s) and 1519 ± 4 (1/s) for the PNS and Rossi-α experiments, respectively. Furthermore, even when multiple detectors were used, DMD provided a unique result for α from all the detector data. Hence, it was confirmed that DMD addressed the issue of the conventional fitting method because it is easy to uniquely determine the fundamental mode component of α.

IV. CONCLUSIONS

Using DMD and randomly sampled virtual data, the present paper attempted to investigate the prompt neutron decay constant α of the fundamental mode component with statistical uncertainty. To demonstrate our proposed technique, experimental analyses by the PNS and Rossi-α methods were performed. In applying the DMD to the PNS and Rossi-α experimental data, the background constant component was removed by adding a constant signal to the experimental data. Consequently, the estimation results for the fundamental mode component of α were approximately constant with respect to the masking time, as compared with the larger variation in the conventional fitting α value. In conclusion, DMD enabled one to robustly estimate the fundamental mode component of α in the PNS and Rossi-α methods, and the applicability of DMD to both methods was demonstrated.

ACKNOWLEDGMENTS

This study has been carried out under the visiting researcher's program at the Kyoto University Institute for Integrated Radiation and Nuclear Science. This study was supported by the Japan Society for the Promotion of Science (JSPS) Grant-in-Aid for Scientific Research (C). [Grant Number 19K05328].

REFERENCES

1. T. ENDO and A. YAMAMOTO, "Data Assimilation Using Subcritical Measurement of Prompt Neutron Decay Constant," *Nucl. Sci. Eng.*, **194**, *11*, 1089 (2020); https://doi.org/10.1080/00295639.2020.1720499.
2. B. E. SIMMONS and J. S. KING, "A Pulsed Neutron Technique for Reactivity Determination," *Nucl. Sci. Eng.*, **3**, *5*, 595 (1958); https://doi.org/10.13182/NSE3-595-608.
3. J. D. ORNDOFF, "Prompt Neutron Periods of Metal Critical Assemblies," *Nucl. Sci. Eng.*, **2**, *4*, 450 (1957); https://doi.org/10.13182/NSE57-A25409.
4. R. KATANO, "Estimation Method of Prompt Neutron Decay Constant Reducing Higher Order Mode Effect by Linear Combination," *Nucl. Sci. Eng.*, **193**, 4, 431 (2019); https://doi.org/10.1080/00295639.2018.1528803.
5. R. KATANO, M. YAMANAKA, and C. H. PYEON, "Application of Linear Combination Method to Pulsed Neutron Source Measurement at Kyoto University Critical Assembly," *Nucl. Sci. Eng.*, **193**, 12, 1394 (2019); https://doi.org/10.1080/00295639.2019.1624084.
6. R. KATANO, M. YAMANAKA, and C.H. PYEON, "Measurement of prompt neutron decay constant with spallation neutrons at Kyoto University Critical Assembly using linear combination method," *J. Nucl. Sci. Technol.*, **57**, *2*, 169 (2020); https://doi.org/10.1080/00223131.2019.1671911.
7. P. J. SCHMID, "Dynamic mode decomposition of numerical and experimental data," *J. Fluid Mech.*, **656**, 5 (2010); https://doi.org/10.1017/S0022112010001217.

8. Z. K. HARDY, J. E. MOREL, and C. AHRENS, "Dynamic Mode Decomposition for Subcritical Metal Systems," *Nucl. Sci. Eng.*, **193**, *11*, 1173 (2019); https://doi.org/10.1080/00295639.2019.1609317.
9. T. ENDO, Y. YAMANE, and A. YAMAMOTO, "Space and energy dependent theoretical formula for the third order neutron correlation technique," *Ann. Nucl. Energy.*, **33**, *6*, 521 (2006); https://doi.org/10.1016/j.anucene.2006.02.002.
10. P. BAETEN, "Heuristic derivation of the Rossi-alpha formula for a pulsed neutron source," *Ann. Nucl. Energy.*, **31**, *1*, 43 (2004); https://doi.org/10.1016/S0306-4549(03)00162-2.
11. T. ENDO et al., "Subcriticality measurement using time-domain decomposition-based integral method for simultaneous reactivity and source changes," *J. Nucl. Sci. Technol.*, **57**, *5*, 607 (2020); https://doi.org/10.1080/00223131.2019.1706658.
12. T. MISAWA, H. UNESAKI, and C. H. PYEON, *Nuclear Reactor Physics Experiments*, Kyoto University Press, Kyoto, Japan (2010).
13. G. R. KEEPIN, *Physics of Nuclear Kinetics*, Addison-Wesley Pub. Co., Inc., Reading, MA (1965).
14. "MCNP User's Manual Code Version 6.2," LA-UR-17-29981, C. J. WERNER, Ed., Los Alamos National Laboratory (Oct. 2017).
15. M. B. CHADWICK et al., "ENDF/B-VII.1 Nuclear Data for Science and Technology: Cross Sections, Covariances, Fission Product Yields and Decay Data," *Nucl. Data Sheets*, **112**, *12*, 2887 (2011); https://doi.org/10.1016/j.nds.2011.11.002.
16. "scipy.optimize.curve_fit — SciPy v1.6.2 Reference Guide," https://docs.scipy.org/doc/scipy/reference/generated/scipy.optimize.curve_fit.html; (current as of Apr. 16, 2021).
17. B. FOAD, A. YAMAMOTO, and T. ENDO, "Uncertainty and regression analysis of the MSLB accident in PWR based on unscented transformation and low rank approximation," *Ann. Nucl. Energy.*, **143**, 107493 (2020); https://doi.org/10.1016/j.anucene.2020.107493.

List of Tables

List of Figures